Insights into the significant increase of ozone during COVID-19 in a typical urban city of China

Kun Zhang [a, b#], Zhiqiang Liu [a, c#], Xiaojuan Zhang [a, c], Qing Li [a, b], Andrew Jensen [d, e], Wen Tan [f], Ling Huang [a, b], Yangjun Wang [a, b], Joost de Gouw [d, e], Li Li [a, b*]

[a] School of Environmental and Chemical Engineering, Shanghai University, Shanghai, 200444, China

[b] Key Laboratory of Organic Compound Pollution Control Engineering, Shanghai University, Shanghai, 200444, China

[c] Changzhou Institute of Environmental Science, Changzhou, Jiangsu, 213022, China

[d] Cooperative Institute for Research in Environmental Sciences, University of Colorado, Boulder, Colorado, 80309, USA

[e] Department of Chemistry, University of Colorado, Boulder, Colorado, 80309, USA

[f] Tofwerk AG, Thun, Switzerland

[#] These authors contribute equally to this work.

Correspondence: Li Li (lily@shu.edu.cn)

Abstract

The outbreak of COVID-19 promoted strict restrictions to human activities in China, which led to dramatic decrease in most air pollutant concentrations (e.g., $PM_{2.5}$, PM_{10}, NO_x, SO_2, and CO). However, obvious increase of ozone (O_3) concentrations was found during the lockdown period in most urban areas of China. In this study, we conducted a field measurement targeting ozone and its key precursors by utilizing a novel proton transfer reaction time-of-flight mass spectrometer (PTR-TOF-MS) in Changzhou, which is representative for the Yangtze River Delta (YRD) city cluster of China. We further applied the integrated methodology including machine learning, observation-based model (OBM), and sensitivity analysis to get insights into the reasons causing the obvious increase of

ozone. Major findings include: (1) By deweathered calculation, we found changes in precursor emissions contributed 1.46 ppbv to the increase in the observed O_3 during the Full-lockdown period in 2020, while meteorology constrained 3.0 ppbv of O_3 in the Full-lockdown period of 2019. (2) By using an OBM model, we found that although significant reduction of O_3 precursors was observed during Full-lockdown period, the photochemical formation of O_3 was stronger than that during the Pre-lockdown period. (3) The NO_x/VOCs ratio dropped dramatically from 1.84 during Pre-lockdown to 0.79 in Full-lockdown period, which switched O_3 formation from VOCs-limited regime to the boundary of NO_x- and VOC-limited regime. Additionally, box model results suggested that the decrease in NO_x/VOCs ratio during Full-lockdown period could increase the MeanO_3 by 2.4 ppbv. Results of this study give insights into the relationship between O_3 and its precursors in urban area, and demonstrate reasons causing the obvious increase of O_3 in most urban areas of China during the COVID-19 lock-down period. This study also underlines the necessity of controlling anthropogenic OVOCs, alkenes, and aromatics in the sustained campaign of reducing O_3 pollution in China.

Keywords: Ozone; VOCs; PTR-TOF-MS; COVID-19

1. Introduction

At the end of 2019, a tragic coronavirus (COVID-19) occurred, which has caused over 271 million global infection and over 4.51 million deaths as of this writing (12th Feb 2022). To protect people's health, China adopted strict measures to control the spread of this pandemic. Thirty provinces, autonomous regions and municipalities have launched Full-lockdown response (also known as Level I response, roughly from 24th Jan to 25th Feb 2020) as early as 24th Jan 2020 (Shen et al., 2021; Li et al., 2020; Huang et al., 2020). With the effective control of COVID-19 in China, the emergency response level in most provinces (except Hubei province, the hardest-hit region) gradually downgraded to Partial-lockdown (Level II and Level III response, roughly after 25th Feb 2020) (Li et al., 2020), and work resumption started. During Full-lockdown period, all the social events that may cause crowds (excluding transportation and industries that maintained the basic operation of society) were severely restricted. Affected by the pandemic, many factories were shut down, and the on-road traffic volume

and construction activities have been reduced significantly (Zheng et al., 2020). During Full-lockdown period, dramatic decrease of air pollutants (e.g., $PM_{2.5}$, NO_2, BC) were found in China, especially in urban areas (Fan et al., 2021; Gao et al., 2021; Li et al., 2020; Xu et al., 2020). Surprisingly, marginal increases of O_3 were observed during the lockdown period in YRD region, and this seems to be contradictory to the decrease of most air pollutants (Li et al., 2020). However, as suggested by previous studies, the formation of O_3 is significantly influenced by NO_x/VOCs ratio and meteorological conditions (temperature, relative humidity and actinic flux) (Zhang et al., 2020a; Zhang et al., 2020b). Therefore, it is essential to investigate the changes of meteorological and emissions conditions to figure out reasons causing the increase of O_3 during this pandemic.

Previous studies on the O_3 pollution in the YRD region have often focused on the more populated metropolitan areas, such as Shanghai and Nanjing, which are considerably far away from the industrial zones that are essentially responsible for the sources of O_3 precursors (Li et al., 2019; Zhang et al., 2020b). Changzhou, located in the center of the Yangtze River Delta (YRD) region, is a typical city with fast urbanization, heavy industrial structure, huge energy consumption, increasing vehicle stocks and frequent air pollution. Therefore, it provides a more representative environment to fully elucidate the mechanism underlying the O_3 pollution in the YRD region (Shi et al., 2020). In a companion paper (Jensen et al., 2021), we also demonstrated that Changzhou is representative for the region by analyzing both surface observations and satellite data. According to previous studies, the anthropogenic VOCs emission in Changzhou was around $9\sim12.6\times10^4$ tons/year, among which industries was the dominant source, accounting for 27~47% of the total VOC emissions (Cheng et al., 2016; Fu et al., 2013). It is notable that industrial sources together contributed over 80% of anthropogenic VOC emissions (Sun et al., 2019). Apart from industrial sources, vehicle exhaust accounted for 9%~14% of total VOC emissions (Sun et al., 2019). However, rare observation regarding VOCs characteristics during COVID-19 in Changzhou has been conducted.

Highly time-resolved measurements of VOCs are generally much sparse and could not be easily expanded during the lockdowns. This limits our understanding of how VOCs changed and how the formation of ozone was affected. Here, we used a novel proton transfer reaction time-of-flight mass

spectrometer (PTR-TOF-MS, Tofwerk, Model Vocus Elf, CHE) to conduct online observation of VOCs in Changzhou. The characteristics of VOCs and the variations of general air pollutants in each emergency response period were analyzed. Additionally, ozone formation during each period was investigated by an OBM model. Although terrifying impact has been caused by the COVID-19, it provided a rare experiment to analyze the variations of VOCs and NO_x due to changes of anthropogenic activities in a typical city of China. Furthermore, results of this study offer theoretical support for formulating refined ozone management policy in China.

2. Methodology

2.1 Field measurement

The field campaign was conducted from 8th Jan to 31st Mar 2020 at a sampling site located on the rooftop of a building at Changzhou Environmental Monitoring Center (CEMC, 31.76° N, 119.96° E), which was approximately 15 m above ground level. As a typical urban monitoring station, this site is in the center of Changzhou city, surrounded by residential and commercial area, which is also adjacent to the main transportation junction in Changzhou (Figure 1). According to local epidemic prevention policies, we roughly classified the measurement periods into three stages: Pre-lockdown (8th January to 23rd January 2020), Full-lockdown (25th January to 24th February 2020), Partial-lockdown (25th February to 28th March 2020) as defined in a study of the Yangtze River Delta (Li Li et al., 2020).

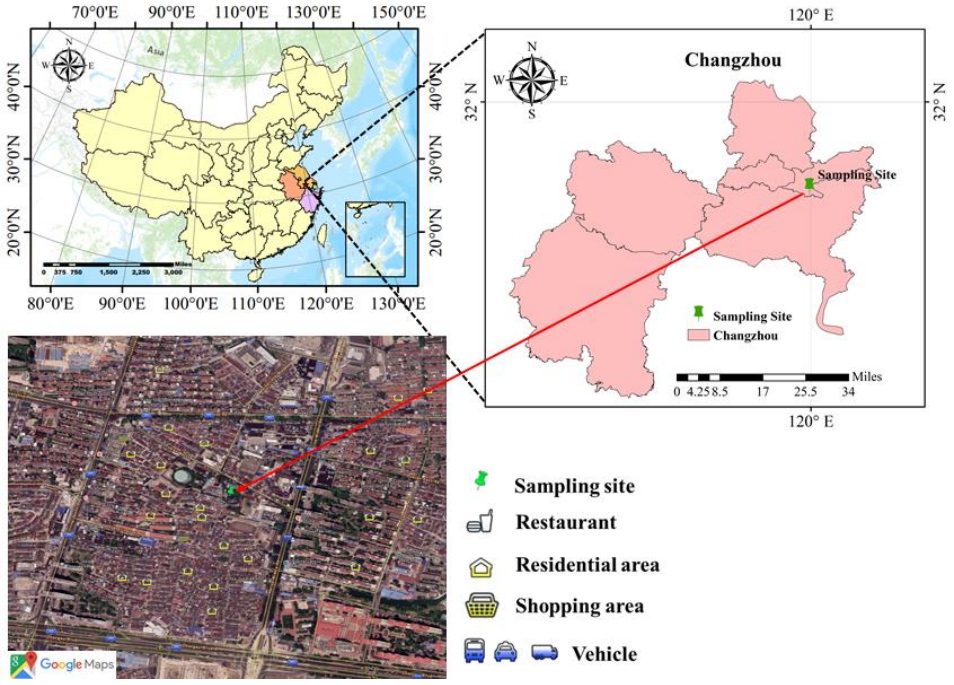

Figure 1. Location of the sampling site in Changzhou.

From Jan 8th to Mar 27th, 2020, the concentrations of traditional air pollutants ($PM_{2.5}$, PM_{10}, NO_x, SO_2, CO, O_3) as well as meteorological parameters were monitored by a series of analyzers (Table 1). In particular, 87 VOCs species were quantified, 59 of which were identified, by a PTR-TOF-MS with time resolution of 1 min. Detailed measurement techniques and quality assurance and control has been documented in detail in our companion paper (Jensen et al., 2021). Here, we just briefly introduce the measurement. The air samples were directly drawn into a 3 m-long tube connected to the instrument. A priming pump, with flow rate of 4 L/min, was used to reduce the retention time of the gas sample in the tube. To avoid blocking of inlet tube caused by particles, a particulate filter was assembled at the front of the inlet tube. The pressure of the ion source was set as 2 mbar and the temperature of the reaction chamber was set to 90 °C during the observation. VOCs are ionized by reactions with H_3O^+ ions from a discharge, and the product ions are detected by a time-of-light mass analyzer (m/Δm FMHW of 950 at m/Q 107). The PTR-TOF-MS can detect most unsaturated hydrocarbons and VOCs with functional groups but cannot detect species with proton affinities lower than that of water, namely alkanes and small alkenes. Eighteen standard gases (including acetonitrile, acetaldehyde, acrolein, acetone, isoprene, butanone, 2-butanone, benzene, 2-pentanone, ethyl acetate, toluene,

methyl isobutyl ketone, styrene, xylene, trimethylbenzene, naphthalene, a-pinene, and 1,3-dichlorobenzene) with concentrations of 1 ppmv were used for the calibration of the PTR-TOF-MS. In addition, a built-in calibration system was used to control the zero and standard gases.

Table 1 Measurements performed during the field campaign.

Species/Parameter	Experimental Technique
T, RH, WS, WD and P	2000WX, Airmax, USA
O_3	400E, API, USA
NO_x (NO and NO_2)	T200, API, USA
SO_2	T100, API, USA
CO	T300, API, USA
$PM_{2.5}$	5030, Thermo Fisher, USA
PM_{10}	5030, Thermo Fisher, USA
VOCs	Vocus Elf, Tofwerk, CHE

2.2 Observation-based model

An OBM model coupled with MCM v3.3.1 was utilized to investigate the atmospheric oxidation capability and the radical chemistry. Detailed information about the chemistry mechanism is available on MCM website (http://mcm.leeds.ac.uk/MCM/, last access 8 Jul 2021). More than 5800 chemical species and 17000 reactions are included in this mechanism. The photolysis frequencies (J values) were calculated as a function of solar zenith angle, altitude using lookup tables, calculated using the Tropospheric Ultraviolet and Visible (TUV) model (Wolfe et al., 2016). Dilution mixing within the boundary layer is considered. However, as a 0-D model, vertical or horizonal transport of airmasses are not involved. The observed meteorological parameters (T, RH, P), trace gases (NO, NO_2, CO, SO_2, and VOCs) were used to constrain the model. Before each simulation, the model was run 3 days as spin-up to reach a stable state. According to the definition of atmospheric oxidation capability (AOC), AOC is quantified by Eq (1) (Geyer et al., 2001).

$$AOC = \sum_{i=1} k_{Y_i-X}[Y_i][X] \quad (1)$$

where Y_i are the primary pollutants (e.g., VOCs, CH_4, and CO); X are atmospheric oxidants (OH, O_3,

NO_3); k_{Yi} are the bimolecular rate constants for the reactions of Y_i and X. A high value of AOC indicates fast scavenge of primary air pollutants. Additionally, OH reactivity (k_{OH}), defined as the reaction rate coefficients multiplied by the concentrations of the reactants with OH, is also widely used as an indicator of AOC. The value of k_{OH} depends on both the abundances and compositions of primary pollutants and can be calculated by Eq (2).

$$k_{OH} = \sum_i k_{OH+X_i} \times [X_i] \quad (2)$$

where k_{OH+Xi} are the reaction rate coefficients of reaction OH+X_i; Xi are the concentrations of pollutants (VOC, NO_2, CO, OVOC etc.) (Zhu et al., 2020).

2.3 Trend Analysis

Mann-Kendall (MK) trend test is a widely used non-parametric test method (Pathakoti et al., 2021; Zhang et al., 2013). It is applicable to all distributions (that is, the data does not need to meet the assumption of normal distribution), but the data should have no serial correlation. If the data has serial correlation, it will have an impact on the significance level (p value). In this study, the MK trend analysis was performed for individual VOC concentrations during Pre-lockdown and Full-lockdown period. By using the "feast" R package, no obvious serial correlation of individual VOC is found. Therefore, the observed VOC data is suitable for MK test. Detailed description and the calculation formula of MK trend test could be found in the study of Pathakoti et al. (2021) and Alhathloul et al. (2021). A positive z value from the MK test indicates increasing trend of the target compound. On the contrary, a negative z value suggests the target compound was decreasing.

Sen's slope, a non-parametric test proposed by Sen (1968), is used in this study to assess the rate of change in individual VOC concentrations. The Sen's slope is selected since it is insensitive to outliers, and does not require a normal distribution of residuals. Sen's slope (Q) is mathematically represented by the following equations.

$$Q = median(SS_{ij}) \quad (3)$$

$$SS_{ij} = \frac{x_j - x_i}{j - i}, 1 \le i \le j \le n \quad (4)$$

where x_j and x_i are concentrations of VOC specie x at time *j* and *i* ($1 \le i \le j \le n$), respectively. SS_{ij} is the linear slope between time *i* and *j*, and Q is the median of SS_{ij}. Positive and negative Q values indicate increasing or decreasing trend of VOC specie x, respectively.

2.4 Deweathered model

The observed concentrations of O_3 could be influenced by meteorological conditions, emissions and/or chemistry. The emissions and chemistry are being treated together and separated from meteorology by the deweathered approach based on the random forest (RF). Hourly data of Unix date (number of seconds since 1970-01-01), Julian day, weekday, hour of day, wind speed (WS), wind direction (WD), temperature (T), relative humidity (RH), and pressure (P), which are available during the whole observation, were used for the deweathered calculation of O_3. The missing data was replaced by linear interpolation. Training of the models was conducted on 80% of the input data and the other 20% was withheld from training. To avoid the disadvantage of overfitting during the training of RF, a process called bagging (or bootstrap aggregation) was adopted. Bagging results in new, sampled set called out-of-bag (OOB) data. A decision tree is then grown on the OOB data. Therefore, all the decision trees are grown on different observations and avoid the overfitting (Grange and David (2019)). To determine the value of number of trees (ntree), number of samples (nsample), and the minimal node size, a series of random forests were performed under different choices of ntree, nsample, and minimal node size. The results suggest that the highest coefficient of determination (R^2, 0.84) was obtained when ntree, nsample and minimal node size was set as 300, 300, and 5, respectively (Table S1 and S2). More details of this model could be found in the study of Grange and David (2019). The uncertainty of the deweather model is obtained by growing 50 random forest models with the hyperparameters described above, which is the same method as Grange and Carslaw (2019). The mean and standard error of the predicted O_3 concentrations is shown in Figure S1, and results of the model are stable during the 50 runs. The differences in observed O_3 concentrations ($O_{3,Obs}$) and deweathered O_3 concentrations ($O_{3,Normal}$) were regarded as the concentrations contributed by meteorology ($O_{3,Met}$), which is consistent with the definition in Li et al. (2021). Correspondingly, the differences in $O_{3,Normal}$ concentrations in different periods represent the influence of emissions,

since the $O_{3,Normal}$ has already removed the influence of meteorological conditions.

3. Results and discussion

3.1 Overview of the field campaign

Figure 2 shows the meteorological conditions during the observation. During the whole experiment, the prevailing WD was southeast. The average T and RH was 9.9 ± 5.1℃ and 58.9 ± 17.1%, respectively. Compared to Pre-lockdown period, the concentrations of $PM_{2.5}$, PM_{10}, SO_2, NO, NO_2, TVOC and CO during Full-lockdown period decreased by 48%, 42%, 11%, 65%, 58%, 33% and 39%, respectively. It should be noted that the decreasing ratio of VOC/NO_x is around 1.75, suggesting that the lockdown policy has stronger influence on NO_x emissions than VOC emissions. The O_3 concentrations during the same period in 2020 and 2019 are summarized in Table 2. Considering the influence of Chinese New Year, the corresponding period in 2019 was decided according to lunar calendar. It should be noted that, compared to Full-lockdown period in 2019, the mean O_3 concentration in 2020 is obviously higher (5.5 ppbv, Figure 2). Meanwhile, the average O_3 concentrations in Full-lockdown period in 2020 was 67% higher than that during Pre-lockdown period in 2020. To roughly analyze the cause of the obvious increase of O_3 during Full-lockdown period in 2020, we summarized the temperature (T) and relative humidity (RH) in Table 2. The T and RH in Full-lockdown period in 2020 was ~1.6 °C higher and 6.1% lower than that in the same period in 2019, while the P and WS were comparable during the same period in 2020 and 2019 (Table 2). The relatively higher T was in favor of O_3 formation during the Full-lockdown period in 2020. As for RH, the influence on O_3 is nonlinear (Zhang et al., 2020), and based on our sensitivity test, lower RH could lead to decrease or increase of O_3 concentration (Figure S2). Overall, changes in O_3 concentrations could be a result of the joint effect of meteorological conditions and emissions/chemistry, the following sections would discuss these influences respectively.

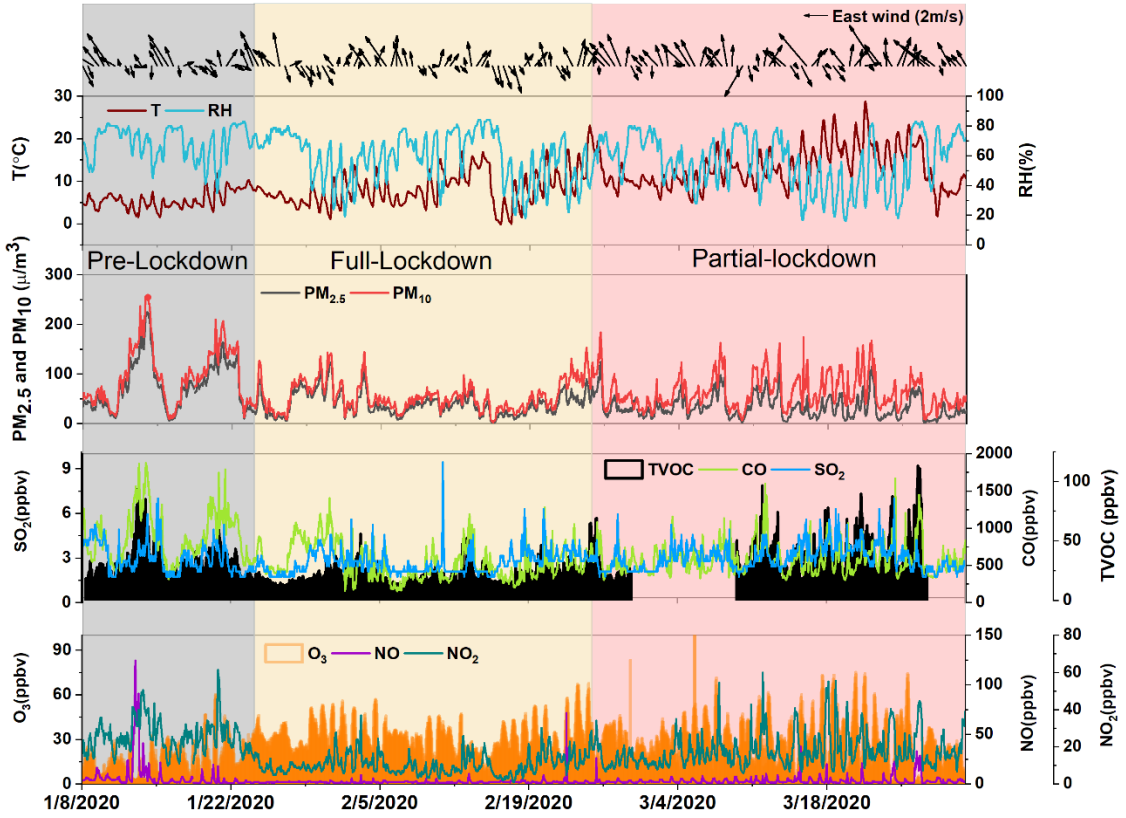

Figure 2 Time series of meteorological parameters and air pollutants during the whole observation.

Table 2 Comparison of average meteorological conditions during Pre-lockdown, Full-lockdown, and Partial-lockdown in 2020 and the same period in 2019.

Periods	Date	P (hPa)	RH (%)	T (℃)	Precipitation (mm)	WS (m/s)
Pre-lockdown	(2020.1.8-1.24)	1025.4	84.9	4.8	0.13	1.8
Same period in 2019	(2019.1.19-2.4)	1025.6	72.7	5.2	0.05	1.9
Full-lockdown	(2020.1.25-2.24)	1025.6	73.0	7.3	0.09	2.1
Same period in 2019	(2019.2.5-3.7)	1024.1	79.1	5.7	0.15	2.1
Partial-lockdown	(2020.2.25-3.31)	1018.9	69.5	12.1	0.11	2.4
Same period in 2019	(2019.3.8-4.12)	1017.6	64.0	13.8	0.02	2.0

3.2 Mechanism affecting the obvious O_3 increase

3.2.1 Meteorological perspective

Deweathered O_3 concentrations were calculated based on the model described in Section 2.4. The difference between $O_{3,Obs}$ and $O_{3,Normal}$ can be regarded as the meteorological influence ($O_{3,Met}$). In

addition, the difference between $O_{3,Normal}$ concentrations in different years could be considered as the influence of emissions ($O_{3,Emi}$). Figure 3 exhibited the average $O_{3,Obs}$, $O_{3,Normal}$, $O_{3,Met}$ during the same periods in 2019 and 2020, respectively. It is obvious that the $O_{3,Obs}$ during Pre-lockdown period is much lower than that during Full-lockdown period in both years, which was partly attributed to negative influence of meteorological condition during Pre-lockdown period (Figure 3). This is consistent with the increasing temperature and solar radiation, which could significantly contribute to the increase in ozone concentration, from Pre-lockdown to Full-lockdown period. It should be noted that meteorology constrained O_3 concentrations by 3.9 ppbv during the Full-lock down period in 2019. Apart from the influence of meteorological condition, the $O_{3,Normal}$ in Full-lockdown period in 2020 is still 1.46 ppbv and 0.64 ppb higher than that during Full-lockdown period in 2019 and that during Pre-lockdown period in 2020, indicating that improper decline of precursor emissions was possibly the key reason for the obvious increase of O_3 during Full-lockdown period in 2020.

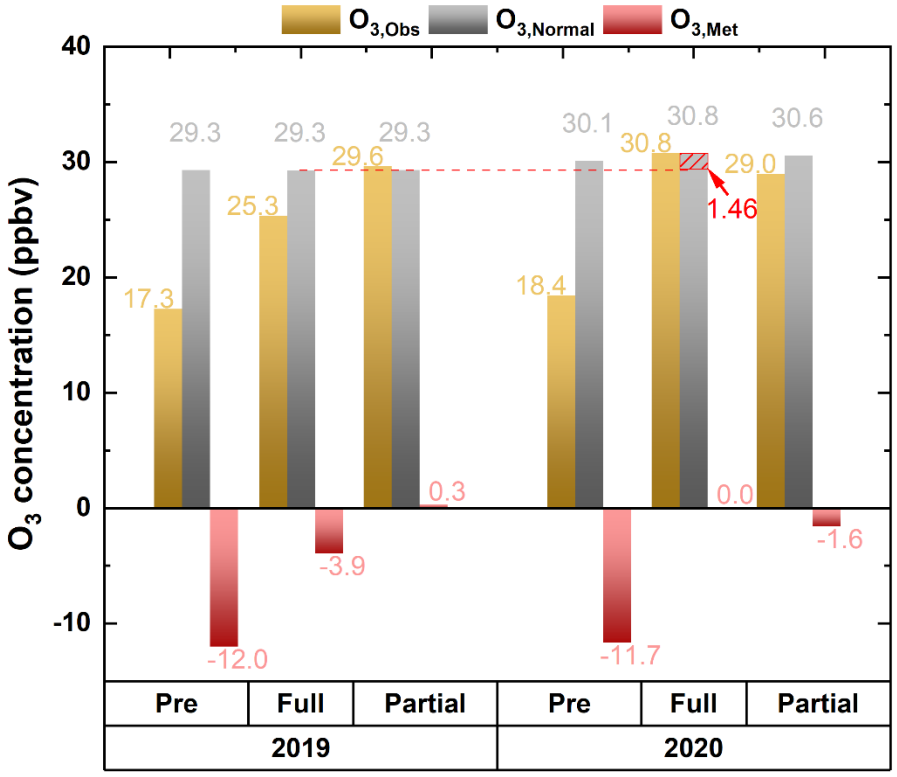

Figure 3. Comparison of observed (Obs), weather-normalized (Normal), and meteorological-factors-infected

(Met) O_3 concentrations during the same period in 2019 and 2020.

3.2.2 Ambient VOCs

As mentioned above, the changes in O_3 precursor emissions strongly affected the $O_{3,Obs}$, and the changes in VOCs and NO_x emissions would eventually be reflected by the observed concentrations of individual VOCs and NO_x. Therefore, the concentrations of each VOC group in different periods were summarized (Figure 4). OVOCs dominated the total VOCs (TVOC) concentrations during the whole observation, with a daily average concentration of 21.44 ± 10.27 ppbv. During Full-lockdown period, the TVOC dropped to 22.19 ±7.9 ppbv from 32.78 ± 13.81 ppbv, which was mainly affected by the decrease in industrial activities and traffic volume. This is proved by the trend of traffic volume, VOCs emission and traffic/industrial-derived VOCs (Text S1 and Figure S3). In addition, Jensen et al. (2021) found the VOC emissions from most industries in Changzhou share the same "U-shape" trend as our study. The most obvious drop was found in aromatics (~54%), followed by OVOCs (~27%), alkenes (~26%), nitrogen hydrocarbon (~25%), and other VOCs (~21%). Additionally, the discrepancy of daytime and nighttime VOCs concentrations during different periods were compared (Figure 4 (A)). The concentration of each VOCs group exhibited higher values during nighttime, which was caused by the low atmospheric oxidation condition and the low atmospheric boundary layer height (Maji et al., 2020; Valach et al., 2015).

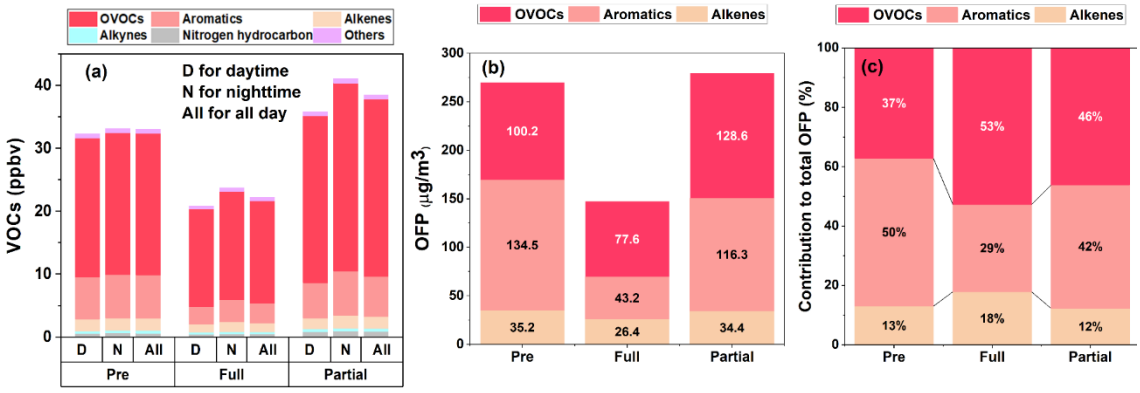

Figure 4. Comparison of daytime and nighttime VOCs concentrations (A), average OFP (B), and contribution to total OFP (C) during different periods.

Furthermore, the average concentrations of individual VOCs during different periods were

summarized in Figure 5. Total 42 VOC species exhibited an 'U' shape trend during the whole observation, while formaldehyde (HCHO) and methanol showed an obvious increasing pattern. It should be noted that the measurement of HCHO could be strongly influenced by humidity. Since within the drift tube, the back reaction, which converse the protonated HCHO back into HCHO, is highly humidity dependent (Inomata et al., 2008; Warneke et al., 2011).

To quantitatively evaluate the changes of individual VOC concentrations from Pre-lockdown to Full-lockdown period, when the variations of each VOCs are obvious, we applied MK trend test and Sen's slope analysis based on the hourly average VOCs concentration data (Table S3). Table 3 lists the top 10 VOCs species with decreasing pattern (with negative Q value) from Pre-lockdown to Full-lockdown period. Toluene, benzene and xylene exhibited the most significant decreasing pattern, with a slope of 7.73×10^{-4}, 7.36×10^{-4}, and 7.20×10^{-4} ppbv h^{-1}, respectively. As for NO_x and TVOC, the slope was -1.62×10^{-2} and $5.48\ 10^{-3}$ ppb h^{-1} (Table S3). This result is consistent with the drastic drop of industrial activities and traffic volumes, which are key sources of aromatics and NO_x, from Pre-lockdown to Full-lockdown period. Other VOCs, such as ethyl-acetate, acetic acid, acetaldehyde, diethyl sulfide, ethanol, butanol and acrolein are also tightly associated with industrial processes, thereby showed decreasing trend from Pre-lockdown to Full-lockdown period. Additionally, the average diurnal variations of acetonitrile, dimethyl formamide (DMF), and styrene, which are tracers of biomass burning and industrial emission, respectively, exhibited significant reduction during Full-lockdown period (Figure S4), also indicating strong decrease in these emissions. However, formaldehyde and methanol exhibited increasing trend, with a slope of 12.78×10^{-4} and 6.35×10^{-4} ppbv h^{-1}, respectively. This could be explained by the secondary formation of HCHO and methanol, which was promoted under better oxidation condition in Full-lockdown period.

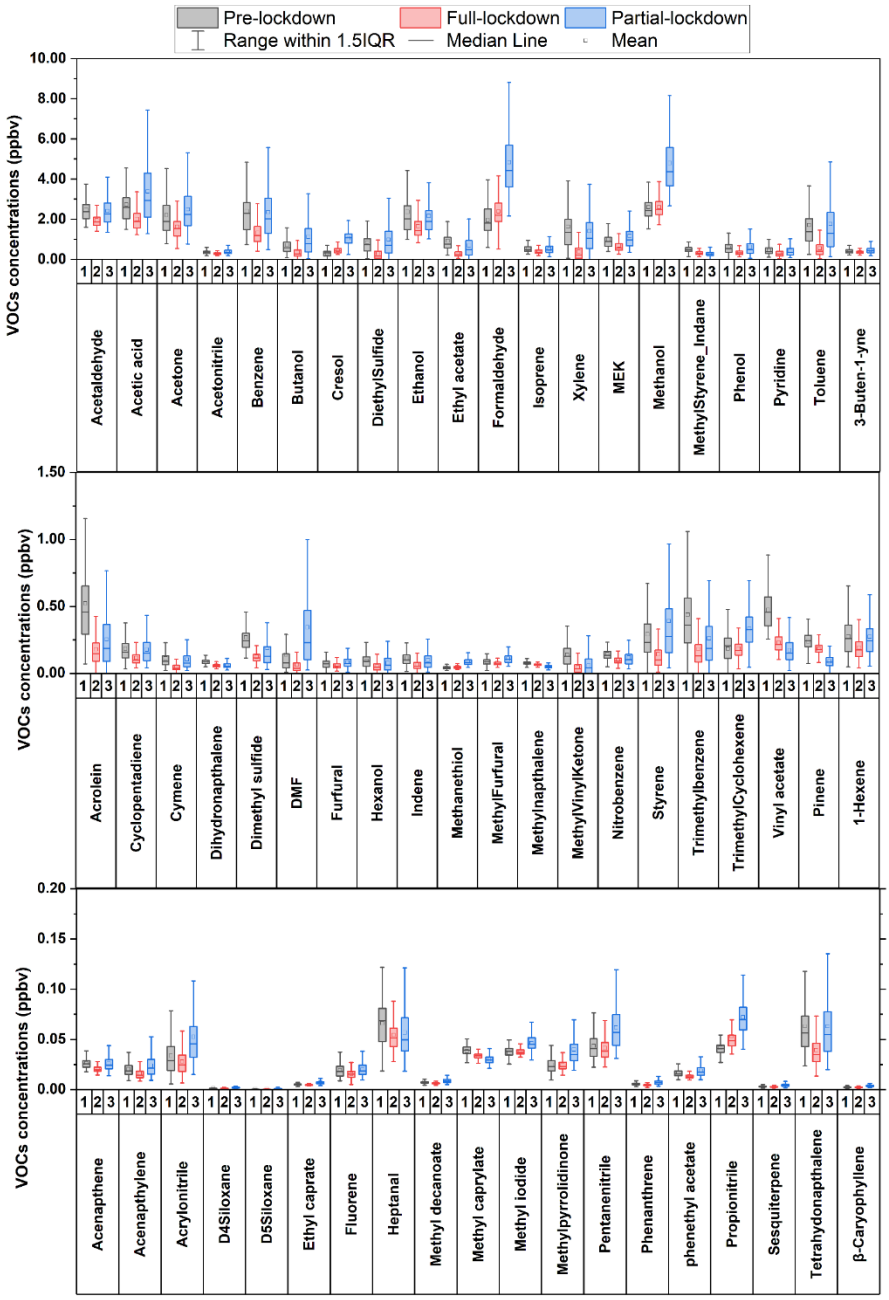

Figure 5. Concentrations of individual VOC species during different period.

***MEK, DMF, are abbreviation of Methyl ethyl ketone and dimethylformamide, respectively.**

Table 3. Top 10 VOCs with decreasing trend from Pre-lockdown to Full-lockdown

VOC	Z value	Q *10000 (ppbv h^{-1})	VOC	Z value	Q *10000 (ppbv h^{-1})
Toluene	-14.02	-7.73	Acetaldehyde	-10.31	-3.95
Benzene	-9.65	-7.36	Diethyl sulfide	-9.15	-3.16
xylene	-12.38	-7.20	Ethanol	-5.48	-3.09
Ethyl-acetate	-18.53	-5.20	Butanol	-10.42	-2.83
Acetic acid	-6.79	-4.12	Acrolein	-15.48	-2.76

3.2.3 Chemistry perspective

The reactivities of different VOCs vary significantly, hence, ozone formation potential (OFP) is used in this study to assess the potential contribution of active VOCs (including alkenes, aromatics and OVOCs) to O_3 formation on the same basis, and it can be calculated by formula (5):

$$OFP_i = MIR_i \times [VOC_i] \quad (5)$$

where MIR_i is the ozone formation potential coefficient for a given VOC species *i* in the maximum increment reaction of O_3, acquired from Carter (2009); $[VOC_i]$ is the concentration of VOC species *i* (in μg/m^3). It should be noted that OFP does not indicate O_3 concentration but only serves as a reference for the potential O_3 produced via the degradation of VOCs. The time series of total OFP is shown in Figure 6. The average OFP in Pre-lockdown, Full-lockdown, and Partial-lockdown period was 269.4 ± 146.0, 147.2 ± 72.4, 279.3 ± 168.6 μg/m^3, respectively. The trend of the total OFP indicates the drastic decrease of VOCs reactivities from Pre-lockdown to Full-lockdown period. During Pre-lockdown period, aromatics were the dominant OFP contributor (49%), followed by OVOCs (38%) and alkenes (13%) (Figure 4). Among VOCs, xylene exhibited the maximum OFP value (68.6 ± 59.3 μg/m^3), followed by acetaldehyde (28.8 ± 6.4 μg/m^3), toluene (25.7 ± 20.1 μg/m^3) trimethylbenzene (25.4 ± 15.8 μg/m^3), and formaldehyde (22.7 ± 9.1 μg/m^3) (Figure S5). Compared to Pre-lockdown period, the OFP of aromatics decreased dramatically (-91.2 μg/m^3) during Full-lockdown period (Figure 4 (B)), which was mainly attributed to the rapid decline of human activities (e.g., transportation and industry). However, the OFP of alkenes and OVOCs only decreased by 8.9 and 22.5 μg/m^3, respectively. During the observation, the most abundant alkenes measured by

PTR-TOF-MS are 1-hexene and isoprene, with the k_{OH} of 37 and 100 $\times 10^{-12}$ cm^3 $molecule^{-1}$ s^{-1} (Atkinson and Arey, 2003), respectively, which are much higher than that of the most abundant aromatics (1.22, 5.63, and 17 cm^3 $molecule^{-1}$ s^{-1} for benzene, toluene, and xylene, respectively). The fast degradation of these alkenes could attribute to the small relatively smaller change of OFP from alkenes. As for OVOCs, the secondary formation could compensate the decrease in primary emissions. The OFP values of aromatics and alkenes during Pre-lockdown and Partial-lockdown period are comparable, but OVOCs exhibited higher OFP contribution (~46%) in Partial-lockdown period, which could be attributed to the higher AOC, enhanced solar radiation and temperature during Partial-lockdown period. To compare the average reactivity of VOCs during different periods, we calculated the mean MIR, derived by dividing the total OFP by total VOC concentration, in each period. A higher MIR means stronger capability of VOCs to produce ozone. As shown in Figure 7, the average MIR during Pre-lockdown, Full-lockdown, and Partial-lockdown period was 3.85, 3.53 and 3.68 (g O_3/g VOC), respectively. This result suggests that VOC species composition in Full-lockdown is more conductive to ozone formation than that in Pre-lockdown, and Partial-lockdown period. However, the formation of O_3 was sensitive to the ratio of NO_x/VOCs and meteorological conditions, which can be significantly different in each period. As shown in Figure 7, the average NO_x/VOCs ratio in the three periods (shown in) was 1.84, 0.79, and 0.84, respectively, suggesting more NO_x was reduced than VOCs during Full-lockdown period, which could further influence the sensitivity of O_3 formation.

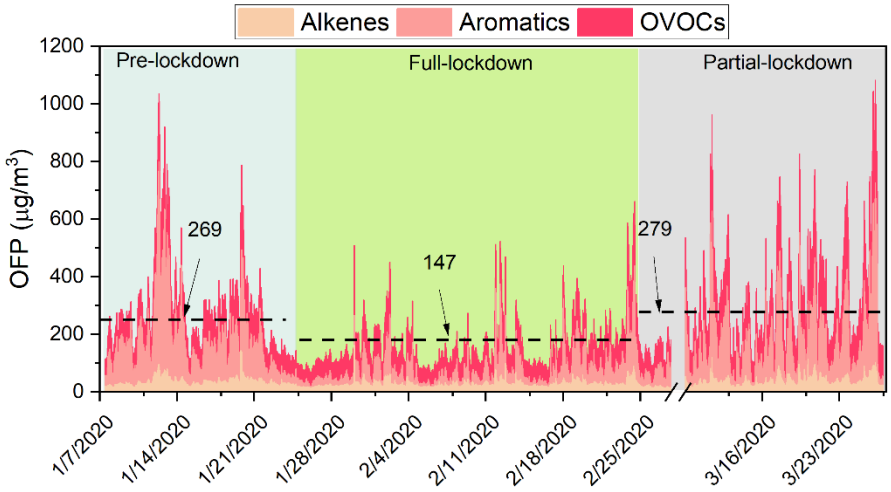

Figure 6. Time series of OFP during the whole observation period (dash lines represent the average OFP value during each period)

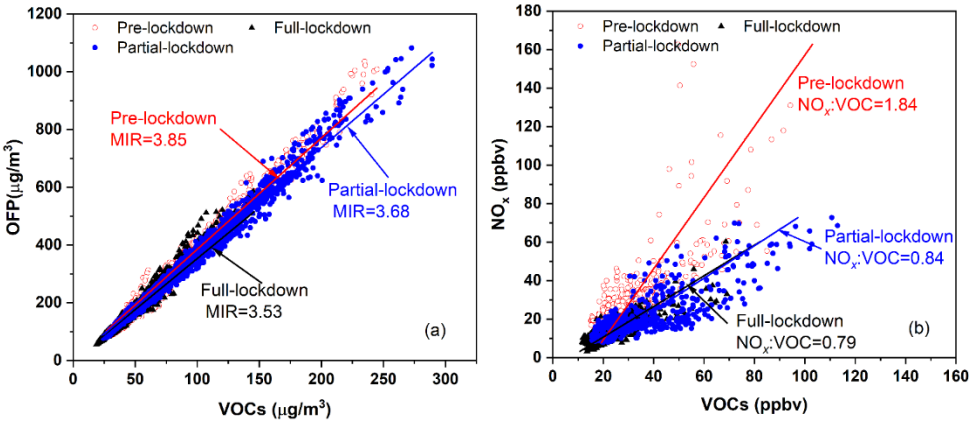

Figure 7. Plot of 1-hour averaged MIR and NO*x* vs VOCs during three periods.

To investigate the detailed formation mechanism of O_3 in each period, three cases (January 19th, February 1st, March 14th) with stagnant meteorological conditions were chosen. The index of agreement (IOA) of O_3 is 0.80, indicating that the model can capture the daytime variation of O_3. The simulated daytime OH concentrations exhibited an increasing trend from January 19th to March 14th, with an average value of $0.36 \pm 0.27 \times 10^6$, $0.75 \pm 0.54 \times 10^6$ and $1.18 \pm 0.78 \times 10^6$ molecules cm^{-3}, respectively. This could be attributed to the increasing solar radiation and temperature from January to March. To analyze the atmospheric oxidation, we calculated the AOC according to Eq(1). The average daytime AOC on Jan 19th, Feb 1st, and Mar 14th was 0.26 ± 0.35, 0.23 ± 0.33, and 0.31 ± 0.38 molecules cm^{-3} s^{-1}, respectively (Figure 9). Comparatively, these values are much lower than those

simulated for Shanghai and Beijing (Liu et al., 2012; Zhu et al., 2020; Zhang et al., 2021) in summer, mainly due to the meteorological conditions in winter season. It is notable that the simulated OH on Jan 19th was significantly lower than that on Feb 1st, but the AOC on Jan 19th was comparable to that on Feb 1st. This should be ascribed to the abundant primary pollutants, which efficiently react with OH, during Pre-lockdown period.

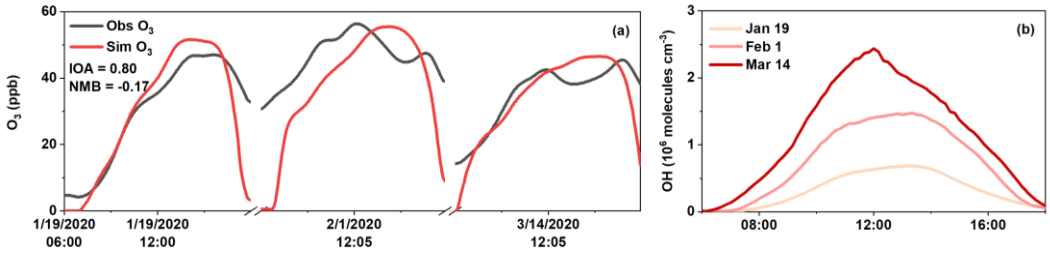

Figure 8. Comparison of simulated and observed O_3 (a) and simulated daytime OH concentrations (b) in three cases.

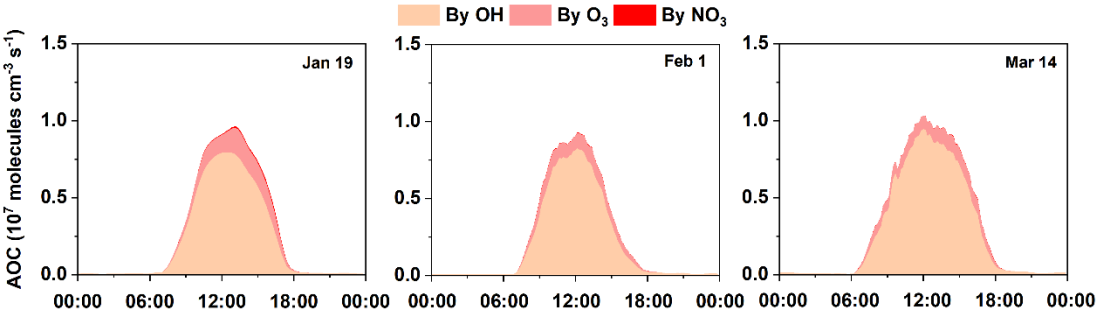

Figure 9. Diurnal variation of AOC in three cases

The daytime variations of OH reactivity calculated by OBM model are exhibited in Figure 10, including the contribution from measured pollutants (e.g., VOCs, NO_x, and CO) and model-simulated species (OVOCs). Generally, the k_{OH} assessed at Changzhou was in the range of 9~32 s^{-1}, which was comparable to that calculated for other cities in China (e.g., Shanghai 4.6~25 s^{-1}, Zhu et al., 2020, Chongqing 15~25 s^{-1}, Tan et al., 2019 and Beijing 15~25 s^{-1}, Tan et al., 2019). It is obvious that OH reactivity peaked in the morning, with maximum values of 31.76, 17.98, and 17.30 s^{-1}, respectively. The OH reactivity from NO_2 exhibited obvious daytime variation, especially during the morning rush

hour, which lead to the peak k_{OH} value during morning. The OH reactivity (k_{OH}) on Feb 1st was much lower than that in the other two cases, which was mainly due to the abundance of emissions during Pre-lockdown and Partial-lockdown period. Compared to Jan 19th, the k_{OH} from NO_2 on Feb 1st and Mar 14th showed lower levels, with an average value of 2.62 and 3.35 s^{-1}, respectively. This corresponds with the dramatic drop of traffic volume during lockdown periods. Similarly, compared to Jan 19th, the k_{OH} from alkenes and aromatics were lower on Feb 1st and Mar 14th. As k_{OH} from OVOC, it shared same trend as OVOC concentration, which reached the minimum value (5.56 s^{-1}) during the Full-lockdown period.

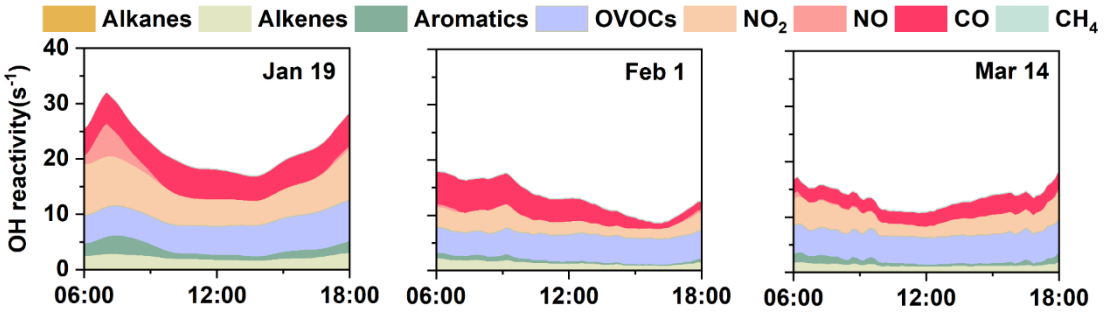

Figure 10. Daytime variation of OH reactivity in three cases

To investigate the variation of O_3 during different periods, the formation and loss pathways of O_3 were calculated (Figure 11). The formation of O_3 ($P(O_3)$) was dominated by HO_2+NO and RO_2+NO pathways. Although the average MIR during Full-lockdown period was the minimum among the three periods, the $P(O_3)$ on Feb 1st was higher than that on Jan 19th. This could be attributed to the higher AOC and better photochemical conditions during Full-lockdown period. Similarly, much higher $P(O_3)$ was found on March 14th. To avoid the influence of meteorological conditions and test the potential mean O_3 ($MeanO_3$) concentrations under different NO_x/VOCs ratios, a series of scenario analyses were performed based on the average condition during the whole observation, and the isopleths of $MeanO_3$ concentrations are exhibited in Figure. 12. Note that the value of temperature and photolysis frequencies (J values) in the scenario analyses could be higher than the actual value during Pre-lockdown period and could further lead to overestimation of simulated $MeanO_3$ during Per-lockdown period. Additionally, the VOCs concentrations mentioned in this section only represent the VOC species in the MCM mechanism. By connecting the inflection points in each O_3 isopleth, we get the

ridge line, which divides the whole regime into NO_x-sensitive and VOCs-sensitive regimes (Figure. 12). During Pre-lockdown period, the O_3 formation was in VOC-limited regime (triangles in Figure. 12), with an average NO_x/VOC ratio of 1.84. As for Full-lockdown period, significant decrease of NO*x* and VOC emissions was observed, and the NO_x/VOCs ratio dropped to 0.79, which gradually switched the O_3 formation to the junction of VOCs-limited and NO_x-limited regimes, especially on Feb 16th and Feb 17th (circles in the red rectangle in Figure. 12), when the O_3 formation went into NO_x-limited regime. During Partial-lockdown period, increasing of VOCs and NO_x emission again dragged the formation of O_3 back into VOCs-limited regime (triangles in Figure. 12). Interestingly, although a great deal of NO_x and VOCs emissions were diminished during Full-lockdown period, the average MeanO_3 in Full-lockdown was supposed to be 2.4 ppbv higher than that in Pre-lockdown period. This result is consistent with the trend of the observed MDA8 O_3 and the results of the deweathered calculation. Therefore, expect for the influence of meteorology, the improper NO_x/VOCs reduction ratio and further influence on chemistry was the key reason for the obvious increase of O_3 during Full-lockdown period in Changzhou in 2020.

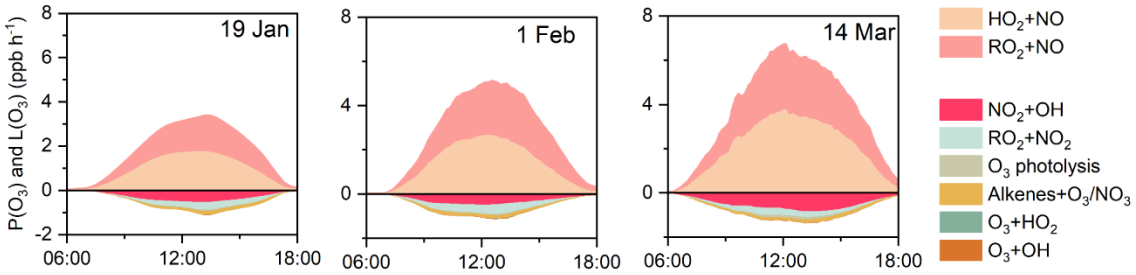

Figure 11**. Daytime variation of P(O_3) and L(O_3) in three cases**

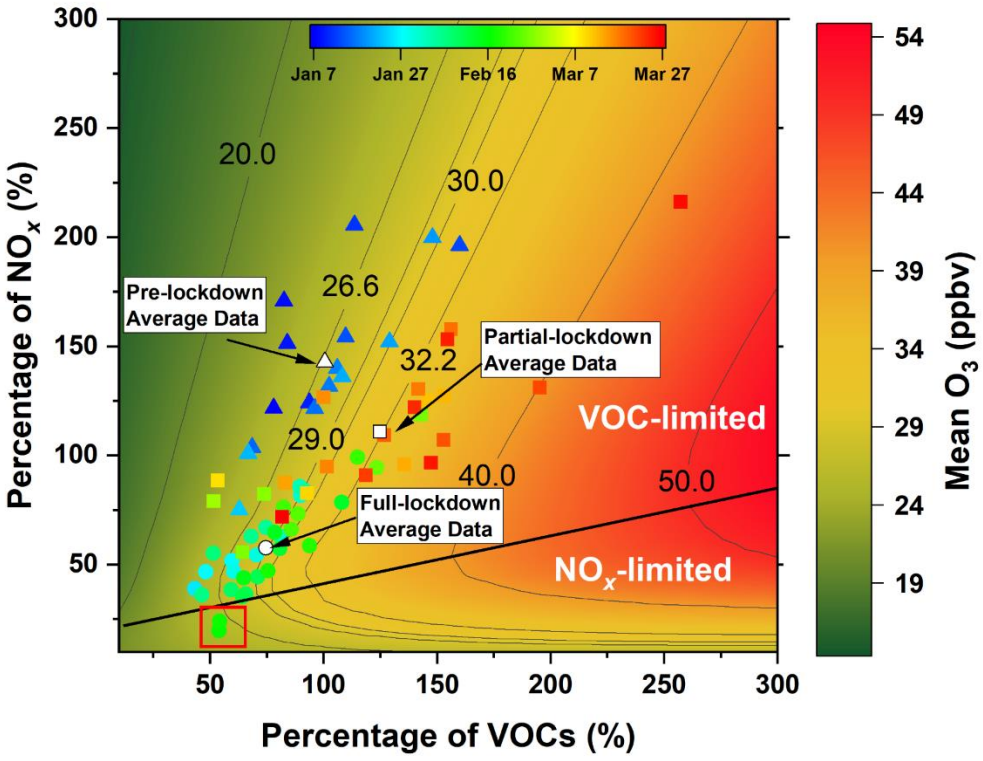

388

389 **Figure. 12 MeanO_3 isopleth. The colored circles, triangles, and rectangles represent the daily average**
390 **concentrations of NO_x and VOCs during Pre lockdown, Full-lockdown, and Partial-lockdown period,**
391 **respectively. The white circle, triangle, and rectangle indicates the average NO_x and VOCs concentrations**
392 **during Pre lockdown, Full-lockdown, and Partial-lockdown period, respectively.**

393 The scenario analyses raise a question: how much O_3 would change as a function of reduction of
394 NO_x and VOCs? Therefore, the reduction percentage of O_3 ($\Delta O_3/O_3$) during Pre-lockdown period as a
395 function of reduction of VOCs and NO*x* were calculated, and the result could be regarded as a
396 potential to control O_3 pollution. Based on the VOCs species in MCM v3.3.1, we classified the
397 measured VOCs into four groups: alkenes (n-butene); aromatics (including benzene, toluene, phenol,
398 xylene, styrene, cresol, and trimethylbenzene); OVOCs (including methanol, ethanol, formaldehyde,
399 aldehyde, acrolein, methyl vinyl ketone, methyl ethyl ketone, ethyl acetate, methyl isobutyl ketone,
400 hexanol, and heptanal); and BVOCs (isoprene, pinene, and caryophyllene). The results in Figure 13(a)
401 indicate that more reduction potential of O_3 could be achieved by diminishing aromatics, followed by
402 BVOCs, OVOCs, and alkenes. It should be noted that many light alkanes and active alkenes, such as

ethene and propene, could not be measured by the PTR-TOF-MS and might further lead to the underestimation of ozone production from alkanes and alkenes. Additionally, this comparison has a drawback of being influenced by the concentrations of VOCs. To normalize the influence of concentrations of VOCs, the descent rate of O_3 (ΔO_3 (ppbv)/ ΔVOCs (ppbv)) as a function of reduction percentage of VOCs were calculated (Figure 13 (b)). O_3 exhibited the highest dependence on BVOCs, with an average descent rate of 3.74 ± 0.09 ppbv/ppbv. Differing from the result in Figure 13 (a), diminishing alkenes could lead to decrease of O_3 by an average declining rate of 1.69 ± 0.01 ppbv/ppbv. On the contrary, reduction of NO_x would lead to increase of O_3, with an average rate of 1.29 ± 0.21 ppbv/ppbv (Figure S6). Although the descent rate of O_3 turned to decrease and the sensitivity of O_3 formation get into NO*x*-limited regime when over 70% of NO_x were eliminated, it still causes net increase of O_3.

Although diminishing BVOCs seems to the most efficient way to restrain O_3 pollution, most of BVOCs were emitted directly from plants and could not be easily controlled. Besides, huge number of OVOCs (such as formaldehyde, aldehyde, methanol, ethanol, methyl vinyl ketone, methyl ethyl ketone, etc.) could be directly emitted from anthropogenic processes or secondary generated from the oxidation of precursors (such as alkenes and aromatics), which complicates the control of OVOCs. Therefore, considering the reduction potential and descent rate of O_3, more efforts are needed on the control of alkenes and aromatics.

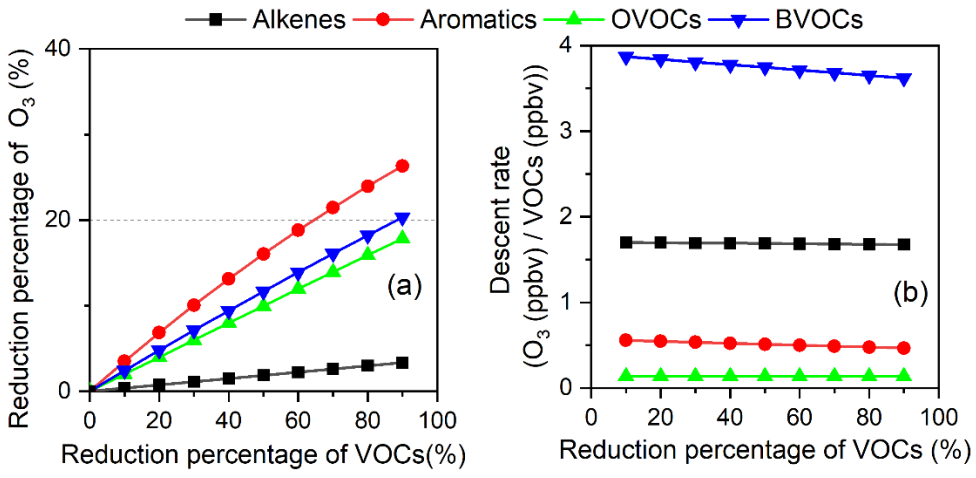

Figure 13. Reduction percentage of O_3 as a function of reduction percentage of VOCs (a); descent rate of O_3 as a

function of reduction percentage of VOCs (b).

3.3 Uncertainty analysis

Due to limitations in the observations, several issues should be noted in the application of the OBM model to evaluate the local chemistry in the present study. Firstly, deficiency of the observation of C2~C5 alkenes and alkanes could lead to underestimation of the simulated O_3. We can only obtain the C2~C5 alkenes and alkanes concentrations from the observation during the autumn of 2018 at the same site. To analyze the uncertainties from this disadvantage, we have done simulation by including assumed diurnal variation of ethene, propene, butene, ethane, propane and butane which are key C2~C5 alkenes and alkanes at this site, in the model. On average, adding 0.5~2 times alkenes or alkanes could lead to 1.65%~9.49% or 1.37~5.36% increase of simulated daytime O_3, respectively (Figure S7 and S8). In addition, the deficiency of C2~C5 has potential to cause uncertainty in O_3 formation potential. To quantify this impact, the EKMA analysis with the hypothetical diurnal variation of C2~C5 was also performed. Generally, adding C2~C5 alkenes and alkanes in the model would lead to increase of the simulated O_3, and could slightly shift the O_3 isopleth to the right without changing the isopleth shape (Figure S9). Therefore, the deficiency of C2~C5 alkenes and alkanes could result in additional uncertainties in O_3 simulation (both time series and EKMA). It should be noted that, this sensitivity analysis is based on the "hypothetical" diurnal variation of C2~C5 alkenes and alkanes, which would bring in uncertainty. We hope a wider range of VOCs would be monitored simultaneously in future field campaign and avoid this deficiency. Secondly, the photolysis frequencies (J values) were calculated as a function of solar zenith angle, altitude using lookup tables, calculated using the Tropospheric Ultraviolet and Visible (TUV) model, which could lead to uncertainty in the simulation of O_3. Hence, we analysis the influence of J values by increasing or decreasing the photolysis rates by 10% and 20%. Results showed that the simulated O_3 could decrease or increase by 25.14% or 21.73%, respectively, when photolysis rates were decreased or increased by 20% (Figure S10). In addition, the J values, which directly or indirectly influence the recycling of RO_x, could lead to uncertainty in the calculation of AOC and k_{OH}. Based on above sensitivity analysis, we

found the relative changes in AOC and k_{OH} by 1% changes in J values was 1.07% and 0.14%, respectively. Therefore, the J values is recommended to be measured during future observations.

4. Conclusions

After the outbreak of COVID-19, strict epidemic prevention measures have been adopted throughout China, leading to dramatic decrease in traffic volume and industrial activities. Affected by the decrease of number of vehicles on the road, non-essential industrial productivity, and associated pollutant emissions, most of the air pollutants (e.g., $PM_{2.5}$, PM_{10}, NO, NO_2, SO_2, and VOCs) dropped to a lower level during lockdown period (especially during Full-lockdown period). However, O_3 increased compared to that during the same period in 2019 in many urban areas of China. To figure out the reasons for this obvious increase of O_3, the characteristics of O_3 precursors (NO_x, VOCs) during Pre-lockdown, Full-lockdown, and Partial-lockdown periods in Changzhou were analyzed. Although this study was conducted in single city of China, the representativeness of Changzhou guaranteed the applicability of the results the YRD region. Results suggested that the decrease of human activities during Full-lockdown period significantly suppressed the emissions of NO_x and VOCs, which further lead to dramatic drop in the concentrations of most VOCs, especially aromatics. As a result, the NO*x*/VOCs ratios dropped from 1.84 at Pre-lockdown period to 0.79 during Full-lockdown period. By deweathered calculation, we found that meteorology constrained O_3 concentration by 3.9 ppbv during Full-lockdown period in 2019, but exhibited negligible influence on that during the same period in 2020. However, compared to Full-lockdown period in 2019, changes in precursor emissions led to 1.46 ppbv increase in O_3 concentrations during the same period in 2020. To verify this result, a box model was used to simulate the formation of O_3. Results show that the AOC level during Full-lockdown was comparable to that during Pre-lockdown period, but the formation rate of O_3 was much higher during Full-lockdown period. By scenario analysis, we found the decrease of NO_x and VOCs in Full-lockdown period dragged the formation of O_3 from VOC-sensitive regime to the junction of VOCs- and NO_x-limited regime, and the average simulated MeanO_3 in Full lockdown period could be 2.4 ppbv higher than that in Pre-lockdown period. Although the

deweathered model and OBM model shows differences in the emission-derived change of O_3, the results together point out that the improper reduction of NO_x and VOCs was the key reason for the obvious increase of O_3 during Full-lockdown period in 2020. Overall, the outbreak of COVID-19 has caused devastation over the world. However, it provided an extreme experiment to investigate the O_3 formation under strict emission control policies and provided insights into the policy formulation for diminishing O_3 pollution in the YRD region. The data indicate that the concentrations of VOCs and NO_x have changed dramatically during the pandemic, a common situation also found in other Chinese cities, and led to the switch of O_3 formation sensitivity. These results have a clear indication that, in the future, more efforts should be paid on the reduction ratio of anthropogenic VOCs and NO*x*.

Acknowledgement

This study was financially sponsored by the National Natural Science Foundation of China (grant 42075144, 41875161, 42005112), and the Shanghai Sail Program (no. 19YF1415600).

References

Alhathloul, SH., Khan, AA., Mishra, AK.. Trend analysis and change point detection of annual and seasonal horizontal visibility trends in Saudi Arabia. Theoretical and Applied Climatology 2021; 144: 127-146.

Atkinson, R. and Arey, J.: Atmospheric Degradation of Volatile Organic Compounds, Chemical Reviews 2003; 103, 4605–4638.

Jensen, A., Liu, ZQ., Tan, W., Dix, B., Chen, TS., Koss, A., Zhu, L., Li, Li., Gouw, J. Measurements of Volatile Organic Compounds during the COVID-19 Lockdown in Changzhou, China. Geophysical Research Letters 2021.

Carter, W. Updated maximum incremental reactivity scale and hydrocarbon bin reactivities for regulatory applications. California Air Resources Board Contract 2009; 339.

Cheng, Z., Zhang, J., Zhou, J., Sun, J., Zhou, W., Chen, C., Zheng, J., Wang, TJ. Air pollutant emission inventory and distribution characteristics in Changzhou (in Chinese). The Administration and Technique of Environmental Monitoring 2016; 28: 24-28.

Fan, L., Fu, S., Wang, X., Fu, Q., Jia, H., Xu, H., Cheng, J. Spatiotemporal variations of ambient air

pollutants and meteorological influences over typical urban agglomerations in China during the COVID-19 lockdown. Journal of Environmental Sciences (China) 2021; 106: 26-38.

Fu, X., Wang, S., Zhao, B., Xing, J., Cheng, Z., Liu, H., Hao, J. Emission inventory of primary pollutants and chemical speciation in 2010 for the Yangtze River Delta region, China. Atmospheric Environment 2013; 70: 39-50.

Gao, C., Li, S., Liu, M., Zhang, F., Achal, V., Tu, Y., Zhang, S., Cai, C. Impact of the COVID-19 pandemic on air pollution in Chinese megacities from the perspective of traffic volume and meteorological factors. Science of The Total Environment 2021; 773: 145545.

Geyer, A., Alicke, B., Konrad, S., Schmitz, T., Stutz, J., and Platt, U. Chemistry and oxidation capacity of the nitrate radical in the continental boundary layer near Berlin, Journal of Geophysics Research 2001; 106, 8013–8025.

Huang, L., Liu, Z., Li, H., Wang, Y., Li, Y., Zhu, Y., Ooi, M., An, J., Shang, Y., Zhang, D., Chan., A., Li, L. The Silver Lining of COVID-19: Estimation of short-term health impacts due to lockdown in the Yangtze River Delta Region, China. GeoHealth 2020; 4: e2020GH000272.

Inomata, S, Tanimoto, H, Kameyama, S., Tsunogai, U., Irie, H., Kanaya, Y., Wang, Z. J. A. C., and Physics: Determination of formaldehyde mixing ratios in air with PTR-MS: laboratory experiments and field measurements, 8, 273-284, 2008.

Li, L., An, J., Huang, L., Yan, R., Huang, C., and Yarwood, G. Ozone source apportionment over the Yangtze River Delta region, China: Investigation of regional transport, sectoral contributions and seasonal differences, Atmospheric Environmental 2019; 202, 269–280.

Li, L., Li, Q., Huang, L., Wang, Q., Zhu, A., Xu, J., et al. Air quality changes during the COVID-19 lockdown over the Yangtze River Delta Region: An insight into the impact of human activity pattern changes on air pollution variation. Science of the Total Environment 2020; 732:139282.

Li, R., Zhao, Y., Fu, H., Chen, J., Peng, M., and Wang, C.: Substantial changes in gaseous pollutants and chemical compositions in fine particles in the North China Plain during the COVID-19 lockdown period: Anthropogenic vs. meteorological influences, 21, 8677–8692, https://doi.org/10/gkgxw6, 2021.

Liu, Z., Wang, Y., Gu, D., Zhao, C., Huey, LG., Stickel, R., et al. Summertime photochemistry during CAREBeijing-2007: RO*x* budgets and O_3 formation. Atmospheric Chemistry and Physics 2012; 12:

7737-7752.

Maji, S., Beig, G., Yadav, R. Winter VOCs and OVOCs measured with PTR-MS at an urban site of India: Role of emissions, meteorology and photochemical sources. Environmental Pollution 2020; 258: 113651.

Pathakoti, M., Santhoshi, T., Aarathi, M., Mahalakshmi, DV., Kanchana, AL., Srinivasulu, J., et al. Assessment of Spatio-temporal Climatological trends of ozone over the Indian region using Machine Learning. Spatial Statistics 2021; 43: 100513.

Sen, PK. Estimates of the regression coefficient based on Kendall's tau. Journal of the American statistical association 1968; 63: 1379-1389.

Shen, L., Zhao, T., Wang, H., Liu, J., Bai, Y., Kong, S., et al. Importance of meteorology in air pollution events during the city lockdown for COVID-19 in Hubei Province, Central China. Science of the Total Environment 2021; 754, 142227.

Shi, X., Ge, Y., Zheng, J., Ma, Y., Ren, X., and Zhang, Y. Budget of nitrous acid and its impacts on atmospheric oxidative capacity at an urban site in the central Yangtze River Delta region of China, Atmospheric Environment 2020; 238.

Sun, K., Zhou, J., Ding, H., Chen, X., Liu, Z., Xue, P. Anthropogenic source VOCs emission inventory of Changzhou city (in Chinese). Environmental Monitoring and Forewarning 2019; 11: 57-62.

Tan, Z., Lu, K., Jiang, M., Su, R., Wang, H., Lou, SR., et al. Daytime atmospheric oxidation capacity in four Chinese megacities during the photochemically polluted season: a case study based on box model simulation. Atmospheric Chemistry and Physics 2019; 19: 3493-3513.

Valach, AC., Langford, B., Nemitz, E., Mackenzie, AR., Hewitt, CN. Seasonal and diurnal trends in concentrations and fluxes of volatile organic compounds in central London. Atmospheric Chemistry and Physics 2015; 15: 7777-7796.

Venter, ZS., Aunan, K., Chowdhury, S., Lelieveld, J. COVID-19 lockdowns cause global air pollution declines. Proceedings of the National Academy of Sciences of the United States of America 2020; 117: 18984-18990.

Wang, W., Li, X., Shao, M., Hu, M., Tan, T. The impact of aerosols on photolysis frequencies and ozone production in Beijing during the 4-year period 2012–2015. Atmos. Chem. Phys. 19, 9413-9429 (2019).

Wang, W., Parrish, D., Li, X., Shao, M., Zhang, Y. Exploring the drivers of the increased ozone production

in Beijing in summertime during 2005–2016. Atmos. Chem. and Phys. 20, 15617-15633 (2020).

Warneke, C., Veres, P., Holloway, J., Stutz, J., Tsai, C., Alvarez, S., Rappenglueck, B., Fehsenfeld, F., Graus, M., and Gilman, J. J. A. M. T.: Airborne formaldehyde measurements using PTR-MS: calibration, humidity dependence, inter-comparison and initial results, 4, 2345-2358, 2011.

Wolfe, GM., Marvin, MR., Roberts, SJ., Travis KR, Liao J. The Framework for 0-D Atmospheric Modeling (F0AM) v3.1. Geoscientific Model Development 2016; 9: 3309-3319.

Xu, L., Zhang, J., Sun, X., Xu, S., Shan, M., Yuan, Q., et al. Variation in concentration and sources of black carbon in a megacity of China during the COVID-19 pandemic. Geophysical Research Letters 2020; 47: e2020GL090444.

Zhang, D., Cong, Z., Ni, G. Comparison of three Mann-Kendall methods based on the China's meteorological data. Advances in Water Science 2013; 24: 490-496.

Zhang, K., Huang, L., Li, Q., Huo, J., Duan, Y., Wang, Y., Yaluk, E., Wang, Y., Fu, Q., and Li, L.: Explicit modeling of isoprene chemical processing in polluted air masses in suburban areas of the Yangtze River Delta region: radical cycling and formation of ozone and formaldehyde, Atmos. Chem. Phys., 21, 5905-5917, 10.5194/acp-21-5905-2021, 2021.

Zhang, K., Li, L., Huang, L., Wang, Y., Huo, J., Duan, Y., et al. The impact of volatile organic compounds on ozone formation in the suburban area of Shanghai. Atmospheric Environment 2020a; 232: 117511.

Zhang, K., Xu, J., Huang, Q., Zhou, L., Fu, Q., Duan, Y., et al. Precursors and potential sources of ground-level ozone in suburban Shanghai. Frontiers of Environmental Science and Engineering 2020b; 14: 1-12.

Zhang, P., Chen, T., Liu, J., Chu, B., Ma, Q., Ma, J., and He, H.: Impacts of Mixed Gaseous and Particulate Pollutants on Secondary Particle Formation during Ozonolysis of Butyl Vinyl Ether, 54, 3909–3919, https://doi.org/10/gpd9p2, 2020.

Zheng, H., Kong, S., Chen, N., Yan, Y., Liu, D., Zhu, B., et al. Significant changes in the chemical compositions and sources of PM2.5 Wuhan since the city lockdown as COVID-19. Science of the Total Environment 2020; 739: 140000.

Zhu, J., Wang, S., Wang, H., Jing, S., Lou, S., Saiz-Lopez, A., et al. Observationally constrained modeling of atmospheric oxidation capacity and photochemical reactivity in Shanghai, China. Atmospheric Chemistry and Physics 2020; 20: 1217-1232.

586